Journal of Marine Research, 48, 701–728, 1990

Retroflection and leakage in the North Brazil Current: Critical point analysis

by G. T. Csanady[1]

ABSTRACT

In an attempt to throw light on the complex flow pattern of the North Brazil Current near its point of separation from the coast, the flow in the neighborhood of boundary- and internal stagnation points ("critical points") has been analyzed. The underlying hypothesis is that fluid masses of widely different potential vorticity come in contact near such points. In a one-and-a-half layer idealization of inertial, frictionless flow the key control parameter is the ratio of potential vorticities of the converging fluids. This determines the angle of flow after separation, and, for given buoyancy and depth scale, the volume of each kind of fluid transported past the stagnation point. A quasi-geostrophic calculation also gives a realistic picture of the streamline field near a stagnation point.

Using the analytical results, a critical point analysis has been carried out on the observed pressure field of the separating North Brazil Current. The results support the idea of direct leakage along the coast into the Guiana Current. They also suggest a second, indirect route of water transport from the North Brazil Current to the North Equatorial Current, via the interior of the cyclonic gyre between the North Equatorial Counter Current and the North Equatorial Current.

1. Introduction

The behavior of Western Boundary Currents is often complex, perhaps in no other place more so than off the North Brazil coast, where the North Brazil Current (NBC) performs its seasonal antics, alternating between continuation into the Guiana Current and retroflection into the North Equatorial Counter Current (NECC). Apart from its changing preferences between eastward or westward continuation, the NBC, as other boundary currents, is attended by a parade of cyclonic and anticyclonic eddies. The flow pattern in the region of NBC retroflection is so complex that even some of its gross features have only been recognized recently.

Similar complexities are encountered in other branches of fluid mechanics, notably in aerodynamics, relating to airflow over the wings of high-speed aircraft, which is subject to three-dimensional separation. In such situations, "critical point analysis" has been helpful in interpreting observations (Perry and Chong, 1987). Critical points

1. Old Dominion University, Department of Oceanography, Norfolk, Virginia, 23529-0276, U.S.A.

are flow singularities, such as interior stagnation points. Identifying such points, and analyzing the flow in their neighborhood yields valuable clues to the large-scale flow pattern.

In oceanography critical point analysis has not been tried, but should be worth exploring. On account of earth rotation, such analysis is more complex than in smaller scale flows. The simplest realistic model is one with a single active layer ("one-and-a-half layer model") which may be expected to simulate the surface flow over a sharp thermocline reasonably well. Such a model should give useful insight into the circumstances of NBC retroflection, particularly in regard to the poleward escape of equatorially formed warm water. More generally, a boundary stagnation point model of this kind portrays one possible mechanism of Western Boundary Current separation, brought about by the blocking effect of fluid of higher potential vorticity.

According to current conventional wisdom, the separation of Western Boundary Currents from the coast is associated with the surface outcropping of the thermocline (Veronis, 1981; Parsons, 1969). This is clearly not the only mode of separation: in the separating NBC the thermocline remains totally submerged. Even in such currents as the Gulf Stream only some upper thermocline layers come to the surface, while the Stream as a whole separates, including especially layers colliding with slopewater. In any case, the local dynamics of separation (whether or not accompanied by full upwelling of some isopycnals) remains to be elucidated. Separation due to "blockage" (presence of a higher potential vorticity fluid mass at the coast) is a plausible idea: without claiming it to be the only possible mode of boundary current separation, its details seem worth exploring.

In an earlier study of NBC dynamics (Csanady, 1985, to be referred to as C1) the northward intruding boundary current was supposed to run into a higher potential vorticity "northern" water mass, to be deflected from the coast and turned back. Model calculations were actually made only for the flow approaching the point of retroflection. The existence of a boundary- or interior stagnation point was inferred from such calculations, without investigating whether or how a stagnation point could be maintained in steady flow. The calculations below close this gap and show in detail how a relatively weak opposing flow of high potential vorticity fluid can deflect a more massive boundary current coming from a lower latitude.

2. Inertial flow in a single active layer

Following up on the analysis in C1, a 1-½ layer model will be used to describe the dynamics of flow near a boundary- or internal stagnation point. Internal friction, and driving by local winds will be neglected, on the hypothesis that the pattern of the flow is governed by the inertia of the converging water masses. The underlying conceptual model is that these waters are set in motion in the oceanic interior by the large scale wind field, and that they arrive at a stagnation point, along or near the western boundary, with prescribed energy and potential vorticity. In the neighborhood of

interior- or boundary stagnation points different water masses come into contact. The object of the analysis here is to elucidate the local dynamics of their interaction.

a. Basic Equations. Scaled equations of motion and continuity for steady flow in a 1-½ model are:

$$\begin{aligned} u\frac{\partial u}{\partial x} + v\frac{\partial u}{\partial y} - v &= -\frac{\partial h}{\partial x} \\ u\frac{\partial v}{\partial x} + v\frac{\partial v}{\partial y} + u &= -\frac{\partial h}{\partial y} \\ \frac{\partial (uh)}{\partial x} + \frac{\partial (vh)}{\partial y} &= 0. \end{aligned} \tag{1}$$

Of interest here is flow in the neighborhood of a stagnation point where the active layer depth is H. The depth elsewhere, h, is expressed as a fraction of H. Velocities in Eqs. (1) are fractions of the internal wave speed $C = \sqrt{\epsilon g H}$, where $\epsilon = (\rho_0 - \rho)/\rho_0$ is the proportionate density defect of the active layer. The Coriolis parameter f is taken to be constant in the limited neighborhood of a stagnation point where the flow will be investigated. The scale for horizontal distances x, y in Eqs. (1) is the radius of deformation, $R = C/f$.

Eqs. (1) may be rewritten in the form:

$$\begin{aligned} v(1 + \zeta) &= \frac{\partial B}{\partial x} \\ u(1 + \zeta) &= -\frac{\partial B}{\partial y} \end{aligned} \tag{2}$$

where ζ is vorticity:

$$\zeta = \frac{\partial v}{\partial x} - \frac{\partial u}{\partial y}$$

and B is Bernoulli function:

$$B = h + \frac{u^2}{2} + \frac{v^2}{2}.$$

The continuity equation is satisfied by introducing a transport stream function ψ:

$$uh = \frac{\partial \psi}{\partial y} \qquad vh = -\frac{\partial \psi}{\partial x}. \tag{3}$$

By cross-differentiating Eqs. (2) it is now readily shown that the quantity $P = (1 + \zeta)/h$, potential vorticity, is a function of the streamfunction alone, $P = P(\psi)$.

Expressing the vorticity by substituting the streamfunction in its definition, one arrives at the equation:

$$\zeta = -\frac{\partial}{\partial x}\left(\frac{1}{h}\frac{\partial \psi}{\partial x}\right) - \frac{\partial}{\partial y}\left(\frac{1}{h}\frac{\partial \psi}{\partial y}\right) = P(\psi)h - 1 \tag{4}$$

which may also be written as:

$$\nabla^2\psi - \frac{1}{h}\nabla h \cdot \nabla\psi = -h[P(\psi)h - 1]. \tag{5}$$

This is a differential equation for $\psi(x, y)$, with the depth being implicitly determined by previous equations. One may imagine solving it by prescribing ψ and $P(\psi)$ on the boundary of the region of interest, and then proceeding into the interior. It is, however, necessary to express the layer depth first as a function of ψ.

b. Subcritical flow. From Eqs. (2) it follows that:

$$\frac{dB}{d\psi} = -P(\psi) \tag{6}$$

so that $B(\psi)$ is also prescribed on each streamline as $P(\psi)$ is specified at the boundary. The layer depth h can now be determined from the definitions of B and ψ:

$$B = h + \frac{T^2}{2h^2} \tag{7}$$

where

$$T^2 = \left[\left(\frac{\partial \psi}{\partial x}\right)^2 + \left(\frac{\partial \psi}{\partial y}\right)^2\right] = |\nabla\psi|^2$$

so that T is the magnitude of the transport. With B and T given, Eq. (7) is cubic in h, containing positive definite quantities only. Real roots can only exist if $T^2/2$ is not larger than $Bh^2 - h^3$, an expression having a maximum value of $4B^3/27$:

$$T^2 \leq \frac{8B^3}{27}. \tag{8}$$

An analytical solution for Eq. (7) may be found by the standard method of solving cubic equations, quoted e.g. by Hartree (1958, p. 220), sketched in Appendix 1. One of the three roots for h is negative, one ranges from zero to $2B/3$, as T^2 varies from 0 to $8B^3/27$, another one from B to $2B/3$. The physical significance of the limit $2B/3$ is that at this depth the velocity magnitude $q = \sqrt{u^2 + v^2}$ equals the local internal wave speed, $q = \sqrt{h}$. When the velocity is greater, the depth is less, and the flow is "supercritical." As in compressible flow (see e.g. Cabannes, 1960), or in channel flow

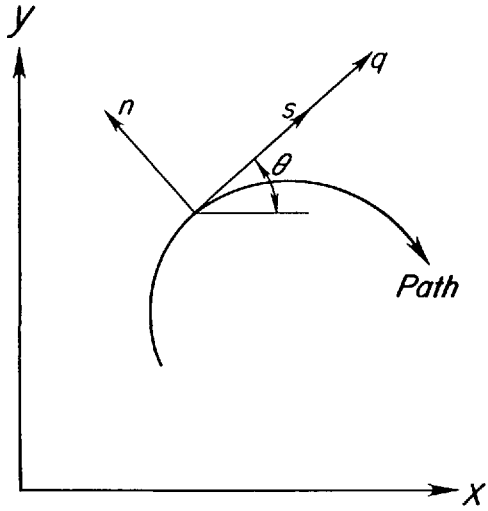

Figure 1. "Natural" coordinates defined by the direction of the velocity vector of magnitude q: s is along the trajectory or streamline, n normal to it, positive n a quarter turn in the direction of positive rotation angle θ.

(Stoker, 1957), a discontinuous transition is possible from supercritical to subcritical flow, (but not vice versa), a "shock" or "internal hydraulic jump." Nof (1986) has recently discussed shocks in a rotating fluid. One certainly cannot exclude the possibility of such shocks in the complex flow region of the NBC. However, in analyzing conditions near a stagnation point it is not necessary to entertain the possibility of supercritical flow, so that only the subcritical root of Eq. (7) will be accepted as realistic:

$$B \geq h \geq \frac{2B}{3}$$

$$h = \frac{B}{3}\left\{1 + 2\cos\left[\frac{1}{3}\cos^{-1}\left(1 - \frac{27T^2}{4B^3}\right)\right]\right\}. \tag{9}$$

Substitution of this result into Eq. (5) yields a very complex equation for the streamfunction: ∇h contains second derivatives of ψ, which are then multiplied by first derivatives. The mathematical character of the problem is therefore not clear, and the integration envisaged from boundaries into the interior cannot a priori be justified.

c. Equations in the (ψ, s) plane. The character of the shallow water equations is clarified by a transformation to natural coordinates s and n, curvilinear coordinates parallel and perpendicular to the velocity vector, see Figure 1 for definitions, the same as in C1. In the present problem an f-plane version of the equations is used, scaled as

above. The velocity vector is specified by its magnitude and direction:

$$q^2 = u^2 + v^2$$
$$\theta = \tan^{-1}(v/u).$$

The flow field is fully described by the three dependent variables q, θ and h. Alternatively, one may use $T = hq$ in place of q. The definitions of ψ, B and T, introduced before imply:

$$\frac{\partial \psi}{\partial n} = hq = T \qquad \frac{\partial \psi}{\partial s} = 0 = \frac{\partial B}{\partial s}$$

so that $\psi = \psi(n)$ only. The normal coordinate n can then be replaced by ψ. The vorticity in natural coordinates is:

$$\zeta = q\frac{\partial \theta}{\partial s} - \frac{\partial q}{\partial n}. \tag{10}$$

Here $\partial\theta/\partial s$ is streamline curvature, $q(\partial\theta/\partial s)$ "curvature vorticity." The equations of motion and continuity may be put into the following form:

$$\begin{aligned} \frac{1}{2}\frac{\partial h^2}{\partial \psi} &= -1 - q\frac{\partial \theta}{\partial s} \\ \frac{\partial h}{\partial s} &= -q\frac{\partial q}{\partial s} \\ \frac{\partial \theta}{\partial \psi} &= \frac{\partial}{\partial s}\left(\frac{1}{T}\right) = -\frac{1}{T^2}\frac{\partial T}{\partial s}. \end{aligned} \tag{11}$$

The first of these expresses cross-stream momentum balance, the second conservation of energy, the third continuity. The first of Eqs. (11) shows that constant depth contours coincide with streamlines only in flow with constant curvature vorticity, i.e. when streamlines are straight or circular. This cannot be the case around a stagnation point.

The above equations fully describe the flow field in the ψ, s plane. The depth h is known as a function of T and ψ from Eq. (9), with $P(\psi)$ and hence $B(\psi)$ prescribed; q follows from the definition of B. From Eq. (7) the ψ-derivative of the depth may be expressed as a function of T:

$$\frac{\partial h}{\partial \psi} = -\frac{1}{3 - 2B/h}\left(P + \frac{T}{h^2}\frac{\partial T}{\partial \psi}\right). \tag{12}$$

Substitution into Eq. (11) leads to:

$$\frac{\partial \theta}{\partial s} = \frac{1}{3 - 2B/h}\frac{\partial T}{\partial \psi} - \frac{h}{T} + \frac{Ph^2/T}{3 - 2B/h}. \tag{13}$$

The angle θ may now be eliminated from Eqs. (11) and (13) by cross-differentiation, resulting in a second-order equation for T. In view of Eq. (12) the form of that equation is:

$$\frac{1}{3 - 2B/h}\frac{\partial^2 T}{\partial \psi^2} + \frac{1}{T^2}\frac{\partial^2 T}{\partial s^2} = \text{funct}\left(\psi, s, T, \frac{\partial T}{\partial \psi}, \frac{\partial T}{\partial s}\right) \tag{14}$$

so that the equation is quasi-linear and elliptic, provided that the flow is everywhere subcritical. The solution of this equation in the (ψ, s)-plane may therefore proceed on conventional lines, through iteration, or integration from prescribed boundary values. The solution yields T, and therefore also h and q. The angle θ is then found by another integration, from Eq. (11) or (13). Streamlines in the x, y plane may be recovered by integrating Eqs. (3).

3. Stagnation point flow model

The question is now, what boundary conditions (if any) to impose on Eq. (5) or (14) in order to produce an interior or boundary stagnation point. Or, from a physical point of view, what is the character of rotational flow in the neighborhood of a stagnation point? Given that the velocity components vanish at a stagnation point, one may try to approach this question by expanding the velocity in a power series, beginning with linear terms in x and y. Goldsbrough (1930) explored this approach, and pointed out that the shallow water equations with rotation possess some exact solutions with the velocities linear, the depth and streamfunction quadratic in the coordinates. These describe motions in a paraboloid, i.e. in a closed basin. Similar exact solutions may be found for an unbounded active layer near a point where the velocity vanishes. They portray streamlines near critical points and lines, and are valuable guides to the interpretation of complex flow patterns. However, they have little relevance to stagnation point flow, as may be seen from a brief review in Appendix 2. The stagnation point type of flow pattern is described by Perry and Chong (1987) as a "saddle." The Goldsbrough expansion for this type of critical point only yields a solution asymptotically valid as $x, y \Rightarrow 0$ and is of little value, see again Appendix 2. In order to find a solution with a wider range of validity, it is necessary to discuss how to prescribe the streamfunction in the inflow and outflow to and from a stagnation point.

a. Geometry of stagnation point flow. An internal stagnation point will be supposed to exist at the confluence of flows from low- and high-potential vorticity regions, where two $\psi = 0$ streamlines cross, see Figure 2 for a schematic illustration. Of the four sectors defined by these streamlines two (1A and 1B) contain high potential vorticity ("southern") fluid, the other two northern fluid. Some sectors may be thought to be parts of large separated eddies, others shoreward extensions of mid-ocean gyres. Taking one half of the diagram away, a boundary stagnation point model is left. In either interpretation, far from the stagnation point the inflow or outflow will be

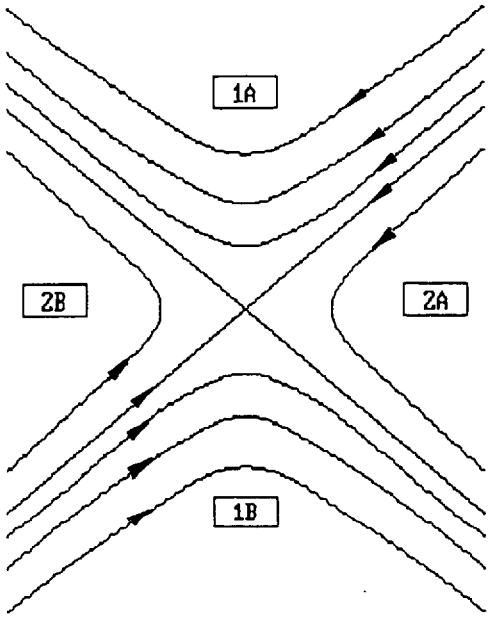

Figure 2. Schematic picture of streamlines around an internal stagnation point, showing alternate anticyclonic (1A and B) and cyclonic (2A and B) regions.

supposed to be geostrophic. In between the inflow and outflow branches, and far from the stagnation point, the potential vorticity will be taken to be constant at $P = P_1$ or $P = P_2$, the total inflow or outflow transport finite at ψ_1 and ψ_2 respectively, the same in opposing sectors. The flow pattern is thus assumed to be symmetric about the $\psi = 0$ streamlines, a possible overidealization of an interior stagnation point. The streamlines in the far field are straight (where the flow is geostrophic). It is plausible to prescribe a straight continuation of the $\psi = 0$ streamlines through the stagnation point matching the near-field solution. It remains to be demonstrated, of course, that a flow pattern of the postulated characteristics can be reconciled with the equations of motion.

If the potential vorticity is supposed constant in each of the separate sectors, the velocity gradient at the separation streamlines becomes discontinuous. In a frictionless model this often has to be accepted. Alternatively, one may make use of the observed fact that gradients of potential vorticity become smoothed ("homogenized") by lateral mixing across potential vorticity fronts. This could be modeled by:

$$P = \frac{P_1 + P_2}{2} + \frac{P_2 - P_1}{2} erf\left(\frac{\psi}{\psi_c}\right). \tag{15}$$

As ψ_c tends to zero, the error function approaches the Heaviside function $\mathcal{H}(\psi)$, reverting to the discontinuous distribution of potential vorticity. In the following

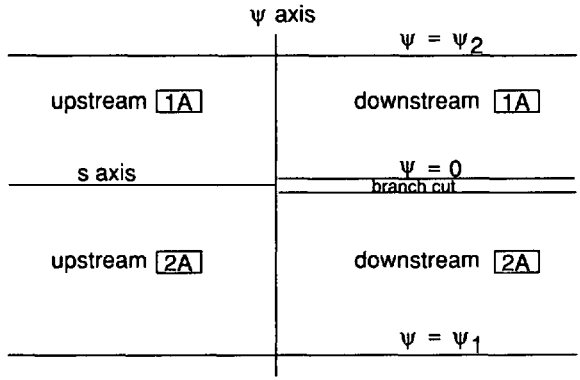

Figure 3. Mapping of the four regions of the previous figure onto an (s, ψ) plane. Quarter planes map onto finite-width strips in the ψ direction, two to a Riemann surface. A branch cut along positive s connects region 1A to 2B, 2A to 1B.

calculations the potential vorticity will generally be taken constant sector by sector. One may think of this as the limiting case of narrow transition zones between sectors.

In the f-plane approach adopted here, with the scaling as specified earlier, the southern fluid is characterized by $P_1 < 1$, $h_1 > 1$ and $\psi_1 < 0$, the northern fluid by $P_2 > 1$, $h_2 < 1$, and $\psi_2 > 0$. It is interesting to see how the pattern of Figure 2 maps onto the ψ, s plane, Figure 3. The upstream half of sector 1A is in contact with the upstream half of sector 2A. However, the downstream halves of these sectors are bounded by sectors 2B and 1B respectively. Moreover, each sector maps onto a bounded strip of a half-plane in ψ, s coordinates. Two Riemann surfaces are therefore necessary in those coordinates, with a cut along the positive s-axis. The stagnation point $s = 0, \psi = 0$ has the character of an essential singularity.

b. The inflow-outflow jets. Far from the stagnation point region, $s \Rightarrow \pm \infty$, the streamlines are supposed to straighten out, θ to become constant. Eqs. (11) imply the following asymptotic relationships as $\theta \Rightarrow$ constant:

$$\frac{\partial T}{\partial s} = 0 \tag{16}$$

$$h^2 = h_0^2 - 2\psi \tag{17}$$

where h_0 is the depth on the separation streamline, $\psi = 0$. On the same streamline the value of the Bernoulli constant is unity, on account of the scaling chosen (the nondimensional depth at the stagnation point was taken to be *one*). With the aid of Eqs. (6) and (17) one may now express the transport as a function of ψ:

$$T = \sqrt{2(h_0^2 - 2\psi)(1 - P\psi) - 2(h_0^2 - 2\psi)^{3/2}}. \tag{18}$$

This equation supplies boundary conditions at infinity on the transport in the (ψ, s) plane. Eq. (17) shows that, as the depth tends to its asymptotic value h_1 or h_2, the streamfunction becomes a maximum or minimum:

$$\psi_1 = (h_0^2 - h_1^2)/2 \qquad \psi_2 = (h_0^2 - h_2^2)/2. \tag{19}$$

On the same limiting streamlines the integrated form of Eq. (6) yields, noting that the velocity magnitude q tends to zero as the depth tends to h_1 and h_2:

$$h_1 = 1 - \psi_1/h_1 \qquad h_2 = 1 - \psi_2/h_2. \tag{20}$$

The last two equations imply:

$$\begin{aligned} h_1 - h_2 &= \psi_2 - \psi_1 \\ h_1 + h_2 &= 2. \end{aligned} \tag{21}$$

The second of Eqs. (21) may be somewhat surprising: in dimensional terms it shows that the scaling depth, chosen to be the depth at the stagnation point, is the arithmetic mean of the asymptotic depths. This follows from geostrophy and constant potential vorticity sector by sector. The asymptotic depths indeed determine all bulk parameters of the flow. Putting $r = h_1/h_2$ (>1 by previous choice of notation) it can readily be shown that:

$$\begin{aligned} h_1 &= 2r/(r+1) \\ h_2 &= 2/(r+1) \\ \psi_1 &= -2r/(r-1)/(r+1)^2 \\ \psi_2 &= 2(r-1)/(r+1)^2. \end{aligned} \tag{22}$$

It may be noted here also that $|\psi_1|/\psi_2 = r$. The depth on the $\psi = 0$ streamline, at large distances $|s|$ from the stagnation point, is:

$$h_0^2 = 4r/(r+1)^2. \tag{23}$$

For subcritical flow h_0 must be greater than $2/3$ because $B = 1$ on the separation streamline. This places a limit on r, $r \leq 6.854$. The bulk relationships deduced here circumscribe the solution $T(\psi, s)$ to a considerable extent. As $\psi \Rightarrow \psi_1$ and ψ_2, T vanishes; as $s \Rightarrow \pm\infty$, Eq. (18) holds. On the $\psi = 0$ streamline, T must be continuous going from one sector to the neighboring one.

c. Momentum integral. An important feature of the large-scale flow pattern envisaged is the deflection of the inflow into the direction of the outflow. Do the asymptotic depths determine also the angle of this deflection? To answer this question consider the control volume shown in Figure 4, between one of the $\psi = 0$ branches (which will now be taken to be the x-axis), perpendicular sections 1 and 2, and a parallel section 3, all except the x-th axis far enough away from the stagnation point. The approaching flow is directed

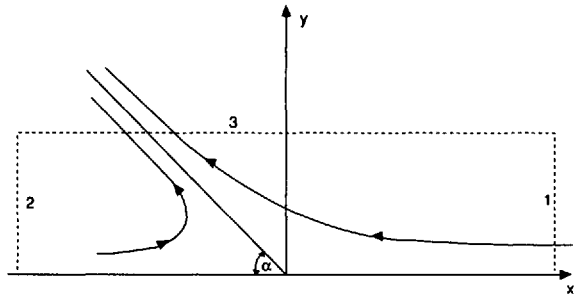

Figure 4. Control volume for the calculation of momentum integrals. All three plane sections (broken lines) are far enough from the stagnation point to be in the geostrophic inflow-outflow. The x-axis is now the separation streamline between regions 1A and 2B, or 1B and 2A.

inward (say) along the axis, out through section 3. Of interest is the integrated momentum balance of the fluid within the control volume, in the x-direction.

Multiplying the first of Eqs. (1) by the depth h, noting the definition of ψ and using the equation of continuity, the area-integral of that equation reduces to the following line-integral along the boundary:

$$\oint [u^2 h\, \mathrm{d}y + uvh\, dx + \psi\, dy + (h^2/2)\, dy] = 0. \tag{24}$$

As noted in a similar analysis by Nof and Olson (1983) and Whitehead (1985), in geostrophic flow the last two terms in the bracket cancel each other out. The first term is nonzero along sections 1 and 2, the second term along 3. Let the integrals along 1 and 2 be written:

$$I_i = \int_0^\infty u^2 h\, dy$$

where i is the number of the section. In virtue of the symmetry of inflow and outflow, the integral along section 3 is readily seen to be, taking account of signs:

$$I_3 = -(I_1 + I_2)\cos\alpha \tag{25}$$

with α being the deflection angle. Eq. (24) therefore becomes:

$$\cos\alpha = \frac{I_1 - I_2}{I_1 + I_2}. \tag{26}$$

The calculation of the integrals I_1 and I_2 may be carried out noting that $|u| = q$, and using Eqs. (16) and (17). The calculation results in:

$$I_i = \frac{\sqrt{P_i}}{6}\left(h_0 - \frac{1}{P_i}\right)^2\left(2h_0 + \frac{1}{P_i}\right) \tag{27}$$

where the index i still denotes the section in Figure 4.

Returning now to the coordinate system used in Figure 2, in which the coordinates bisect the space between the $\psi = 0$ lines, the slope of the x-axis is $m = \tan(\alpha/2)$:

$$m = \tan(\alpha/2) = \sqrt{\frac{1 - \cos\alpha}{1 + \cos\alpha}} = \sqrt{I_2/I_1} \tag{28}$$

where Eq. (26) has been substituted. Using Eqs. (22), (23) and (27), one finds the momentum flux ratio:

$$I_2/I_1 = \frac{1}{\sqrt{r}}\left(\frac{2\sqrt{r} + 1}{2\sqrt{r} + r}\right) \tag{29}$$

a simple enough result characterizing the overall geometry of the stagnation point flow in terms of the depth ratio r alone.

4. Streamline pattern

The net result of the foregoing discussion is that once the depth ratio r is known, the boundary conditions on the inflow are fully specified (assuming of course that the scaling parameters are also known). The task is then to solve Eq. (5) and or (14) subject to these boundary conditions. Unfortunately, neither equation is simple enough to offer any hope of finding an explicit analytical solution. In order to gain an idea of the streamline pattern nevertheless, and also to lay the foundations for a numerical approach, it is plausible to analyze a linearized version of the problem.

a. Quasigeostrophic approximation. Deleting the quadratic term on the left-hand side of Eq. (5), putting $P = 1/h_1$ for the anticyclonic sector, and supposing that depth variations $\Delta h = h - h_1$ are small compared to the rest depth h_1, the right-hand side is seen to equal $-\Delta h$. Small depth changes imply small velocities, so that $\Delta h \approx \Delta B$. From Eq. (6) it follows then that:

$$h - h_1 = P_1(\psi_1 - \psi). \tag{30}$$

Substitution into Eq. (5) yields the quasigeostrophic potential vorticity equation:

$$\nabla^2\psi - P_1\psi = -P_1\psi_1 \tag{31}$$

for sector 1, and the same equation with ψ_2, P_2 in place of ψ_1, P_1 for sector 2. For a boundary current the approximations involved are rather crude. The asymptotic relationships of the previous section show that depth variations are small only if the rest depth ratio r is close to unity, the angle α not too different from 90°. Nevertheless, the solutions of Eq. (31) satisfying appropriate boundary conditions should portray the streamline pattern qualitatively correctly.

The postulated geometry of the flow implies that the streamfunction vanishes along piecewise straight boundaries, enclosing wedges of cyclonically or anticyclonically

turning fluid. In the middle of the wedges, far from the stagnation point, the streamfunction has to remain finite, and tend to ψ_1 or ψ_2, according to sector. These boundary conditions define a unique solution of Eq. (31), sector by sector. However, the physically correct boundary conditions along the separation streamlines are continuity of pressure (and streamfunction), not the specific shape of the boundary surmised on the basis of far-field behavior. In the case of an internal stagnation point both separation streamlines are free streamlines, in the case of a boundary stagnation point, one branch of the separation streamline. Before embarking on the calculation of the solution, it is therefore advisable to investigate whether or how quasigeostrophic solutions for the cyclonic and anticyclonic wedges can be fitted together, to satisfy the pressure continuity condition at their boundary.

The approximation in Eq. (30) implies that the depth on the separation streamlines, $\psi = 0$, is constant. This is of course inaccurate, violating conservation of the Bernoulli function, but the error is of order q^2 and has to be accepted as the price of linearization. On the other hand, continuity of pressure between sectors may be ensured, by prescribing on these streamlines:

$$h_0 = h_1 + \psi_1/h_1 = h_2 + \psi_2/h_2. \tag{32}$$

In spite of the inaccuracy of depth on the separation streamlines, the total transport can be kept the same as required by the exact relationships in section 3:

$$\psi_2 - \psi_1 = (h_1^2 - h_2^2)/2. \tag{33}$$

The last two equations imply the results written down in Eqs. (21) and (22), although with the different separation streamline depth of $h_0 = (h_1 + h_2)/2 = 1$. The split of the total transport between the two sectors also remains in accord with the exact relationships. In other words, quasigeostrophic solutions for wedges, with the streamfunction tending to ψ_1 or ψ_2 far from the boundary, satisfy pressure continuity within their limits of accuracy.

b. Construction of a solution. Eq. (31) may be simplified by absorbing the constant P_1 in the length scale, and ψ_1 in the streamline scale. Writing:

$$x^* = \sqrt{P_1}x, \qquad y^* = \sqrt{P_1}y, \qquad \psi^* = \psi/\psi_1$$

and then dropping the stars on the rescaled variables, Eq. (31) becomes:

$$\nabla^2\psi - \psi = -1. \tag{34}$$

The same equation applies to sector 2, except that the scaling of distances involves P_2, of the streamfunction ψ_2. The obvious particular solution of this equation is $\psi = 1$. The required solution of the homogeneous equation, ψ_h, has to cancel this on the "boundary" (separation streamline), $\psi_h(b) = -1$, and has to tend to zero at large distances from

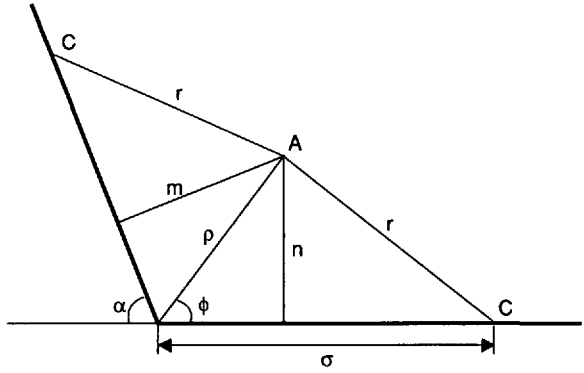

Figure 5. Definition sketch for quantities used in the calculation of the streamfunction at interior points.

that streamline. The "fundamental solution" of the homogeneous equation (Courant and Hilbert, 1962, p. 244) is $K_0(r)$, where K_0 is modified Bessel function, r distance from a "source" (in diffusion, point charge in potential theory). The solution of the homogeneous equation satisfying the boundary conditions can be expressed as the field of a row of doublets arranged along the boundary:

$$\psi_h = \frac{1}{\pi} \int_{-\infty}^{\infty} g(\sigma) \frac{\partial r}{\partial n} K_1(r)\, d\sigma \tag{35}$$

where n is normal distance from the boundary, σ is distance along the boundary, $g(\sigma)$ is doublet strength distribution, and:

$$r^2 = (x - \xi)^2 + (y - \eta)^2$$

with (x, y) the coordinates of the interior point A where ψ_h is calculated, and (ξ, η) those of boundary points C, see Figure 5. The integration must take in the entire boundary, with point C moving first toward the origin, and then away from it on two lines enclosing the angle α for the cyclonic sector, π-α for the anticyclonic sector. The zero of the σ-coordinate is conveniently taken to be the origin O, and the integration split into two segments, along the two straight pieces of the boundary. The derivative of the radius, $\partial r/\partial n$, equals n/r along one segment, m/r on the other (Fig. 5).

The doublet strength distribution must be such as to satisfy the boundary condition, $\psi_h = -1$, along the separation streamline. It is clear from the symmetry of the streamlines about the bisector that $g(\sigma)$ is an even function. Applying Eq. (35) to boundary points the length of one normal vanishes, so that the integrand along one branch of the boundary is zero except where r vanishes, and $K_1(r)$ is singular. The integral for this branch of the boundary equals the value across the singularity, $\pi g(\sigma)$, so that the integral along the entire boundary is:

$$g(\sigma) + \frac{1}{\pi} \int_{-\infty}^{0} g(\sigma') \frac{n}{r} K_1(r)\, d\sigma' = -1. \tag{36}$$

This is an integral equation to be satisfied by the doublet distribution $g(\sigma)$. It is easily solved through an iteration procedure, starting with $g(\sigma') = -1$. The doublet strength at the origin can be found analytically and is, for the anticyclonic sector:

$$g(0) = -\frac{1}{1 + \alpha/\pi}. \tag{37}$$

In the anticyclonic sector, the fourth iteration on Eq. (36) differs little from the third, and is within the accuracy of the integration indistinguishable from an exponential-decay approach to the asymptotic value of $g(\infty) = -1$:

$$g(\sigma) = -1 + \frac{\alpha/\pi}{1 + \alpha/\pi} \exp(-\sigma). \tag{38}$$

It should be possible to verify this result analytically, but it is not clear how. In the cyclonic sector the same approximation does not hold. As written down, Eq. (37) is valid for the anticyclonic sector: in the cyclonic sector α must be replaced by $\pi - \alpha$. Otherwise the doublet distribution on the boundaries of the cyclonic sector is calculated from Eq. (36), as in the anticyclonic sector.

At large distances from the origin one expects the influence of the doublets on the far branch of the boundary to become negligible. Thus if point A in Figure 5 moves parallel to the boundary toward $\sigma = -\infty$, the value of the streamfunction should become a function only of the distance from the boundary, n. Eq. (34) has such a solution, $\psi = \text{const.} \exp(-n)$. The doublet strength distribution tends here to $g(\sigma) = -1$, so that the integral in Eq. (35) should tend to $\exp(-n)$.

The evaluation of this integral is facilitated by a transformation of the integration variable to θ, the angle included between n and r in Figure 5. The relationship between σ and θ is:

$$\sigma = n\{\tan(\theta) - \tan(\phi - \pi/2)\} \tag{39}$$

where $\phi = \tan^{-1}(y/x)$, polar angle. The limits of the integration, $\sigma = 0$ to ∞, change to $\theta = \phi - \pi/2$ to $\pi/2$. On the other branch of the boundary, where the normal has a length of m, σ is calculated from (36) with n replaced by m, $\phi - \pi/2$ by $\phi + \alpha - \pi$. Eq. (35) then transforms into:

$$\psi_h = \frac{1}{\pi}\int g(\sigma)\frac{n}{\cos(\theta)} K_1\left(\frac{n}{\cos(\theta)}\right) d\theta + \frac{1}{\pi}\int g(\sigma)\frac{m}{\cos(\theta)} K_1\left(\frac{m}{\cos(\theta)}\right) d\theta \tag{40}$$

with limits as specified above. This integration may be carried out with great economy of computer time. At large σ, where $g(\sigma)$ tends to its asymptotic value, the integration yields $\psi_h = -\exp(-n)$, within the accuracy of the computations. This agrees with the analytical solution which should asymptotically be valid, but again it is not clear how to reduce the integral to this form.

The calculated streamline field in the neighborhood of a boundary stagnation point is

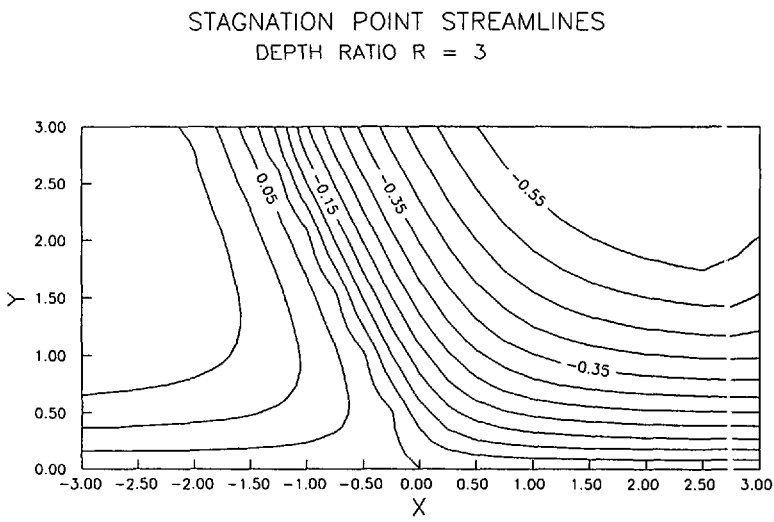

Figure 6. Streamlines in a half plane near a boundary stagnation point, given by the quasigeostrophic solution, for depth ratio $r = 3$. Wiggles near the edges and along the free separation streamline are contouring artifacts. Contour interval is 0.05, and the values of the normalized streamfunction at infinity are 0.25 in the cyclonic sector (left), -0.75 in the anticyclonic one.

shown in Figure 6, for a depth ratio $r = 3$, in Figure 7 for $r = 5$. The wiggles are courtesy of the contouring program. The distances are marked in the original scaling, as multiples of the radius of deformation. The figures illustrate that a relatively feeble cyclonically turning current can block a massive anticyclonically turning flow.

The inaccuracy of the quasigeostrophic solution is greatest along the separation streamlines, at relatively large distances from the stagnation point. Here the normal gradient of the streamfunction (the transport) is discontinuous, on account of the approximation that depth equals Bernoulli function. Given the benign mathematical character of the problem, one expects a relaxation solution to correct this error. With a numerical approach in mind it is worth pointing out that the linearized equation (34) possesses another solution satisfying the boundary condition $\psi = 0$ on the separation streamlines, tending, however, to infinity far from the stagnation point. This solution is written down in Appendix III.

5. Critical point analysis of the North Brazil Current

How can simple analytical models such as discussed above, or in Appendix 2 below, help interpret observations on the complexities of boundary current behavior? The essence of the method to be used, one version of "critical point analysis," is that the potential vorticity of the separate fluid masses present is estimated using the center depth of cyclonic or anticyclonic eddies or gyres, and then constraints on flow around

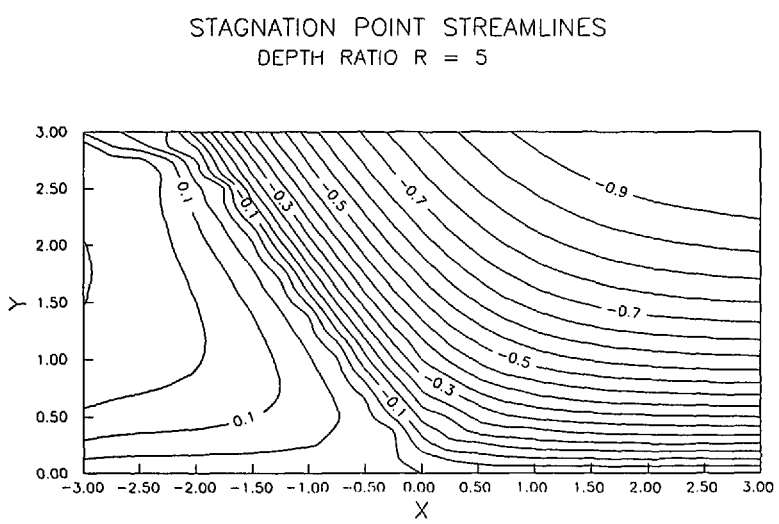

Figure 7. As previous figure, for depth ratio $r = 5$. The change in deflection angle is a direct result of higher inflow momentum flux from the right. The values of the normalized streamfunction at infinity are now 0.2222 to -1.1111.

stagnation points are invoked, to estimate how much of each different water mass is transported past the stagnation points. This method will be applied to the separation region of the NBC. One must state in advance, that given the idealizations of the models applied, the results must not be regarded as absolute truth, only tentative conclusions subject to direct empirical verification. Prior to the application of the method, the observational evidence has to be described first.

a. NBC retroflection and leakage. As mentioned in the introduction, and as discussed in some detail in C1, the NBC separates from the coast around 6–8N, reverses course to the eastward, and its waters join the NECC, in boreal summer and fall. In the remainder of the year, the NBC continues along the coast, becomes the Guiana Current, which eventually joins the North Equatorial Current (NEC) on the westward course of the latter along the north coast of South America. It is usually taken for granted that the seasonal retroflection of the NBC temporarily stops all "leakage" of its waters into the Guiana Current-NEC system. Thus Muller-Karger *et al.* (1988) conclude from an analysis of satellite color images and satellite tracked float data of Richardson and Reverdin (1987), that the NBC seasonally alternates between full deflection into the NECC, and full continuation along the coast to become the Guiana Current. However, the satellite image and float evidence is also consistent with the presence of some leakage in summer, and some eastward flow in winter.

In satellite images taken in boreal summer and fall, dark blue waters of the NBC extend along the shelf-edge to about 7N, the "armpit" of the retroflection. Figure 8

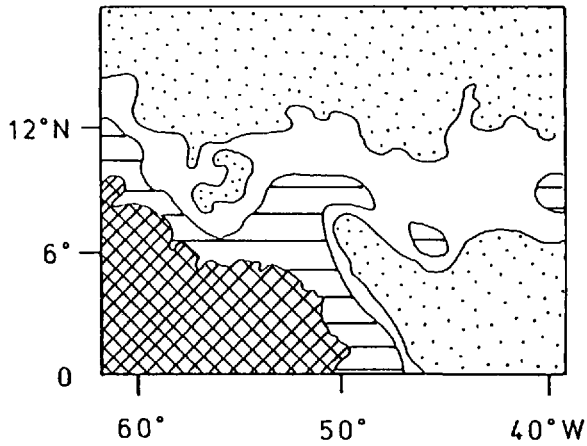

Figure 8. Pigment plume of the Amazon river in boreal summer-fall, traced from satellite image of Muller-Karger *et al.* (1988). The area shaded with horizontal lines is rich in Amazon-derived surface pigment, that with dots devoid of it. The clear area in between is intermediate, containing some river water.

here is a tracing from the composite image of Muller-Karger *et al.*, outlining regions of dark blue ocean waters from the South (− −), orange-green coastal water (+ +), and light blue mixed water (clear). The coastal waters are carried offshore on the cyclonic flank of the separating current, to continue eastward in the NECC. North of the NECC one sees blue deep ocean waters again, but coming from farther North, with the westward drift in a seasonally appearing basin-wide cyclonic gyre between the NECC and the NEC, and in the NEC itself. Southward intrusions of this northern water mass are suggested by the image both to the east and west of the retroflection, in the east showing the long planetary waves of the NECC. It is clear, however that mixed waters are also present west of the retroflection, as far as the Antillean arc, at least to 62W.

The picture for the early months of the year (Fig. 9 here, coded as Fig. 8) is less clear, on account of clouds over the equatorial belt, where the Trade Convergence is located at this time of the year. Nevertheless, a tongue of coastal water clearly reaches northward at about 54W, separate blobs of coastal water are scattered along 9N, while mixed waters extend broadly eastward as well as westward. Muller-Karger *et al.* interpret the eastward extension as a residue from the previous season, when the NECC would have carried coastal water offshore. It is difficult to believe, however, that color is maintained for months, and that marked waters move back into the exact same region where they came from.

b. The pressure field. Two remarkable AXBT surveys of Bruce and Kerling (1984) yielded an approximate synoptic picture of the surface pressure field surrounding the NBC retroflection region in boreal summer and winter. Depth contours of the 20° isotherm, drawn by Bruce and Kerling for boreal winter and summer are reproduced

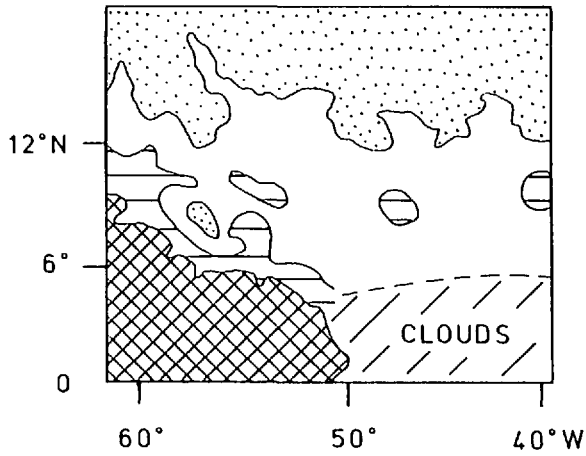

Figure 9. As Figure 8, in boreal winter, coding the same.

here in Figures 10 and 11. As Bruce *et al.* (1985) emphasize, there is considerable general similarity in the summer and winter flow patterns, especially in regard to the eddy field. Furthermore, alongshore hydrographic sections from ships of opportunity (Bruce, 1987) and the few extant area-wide hydrographic studies show that these patterns recur year after year with only minor variations. A large anticyclonic eddy

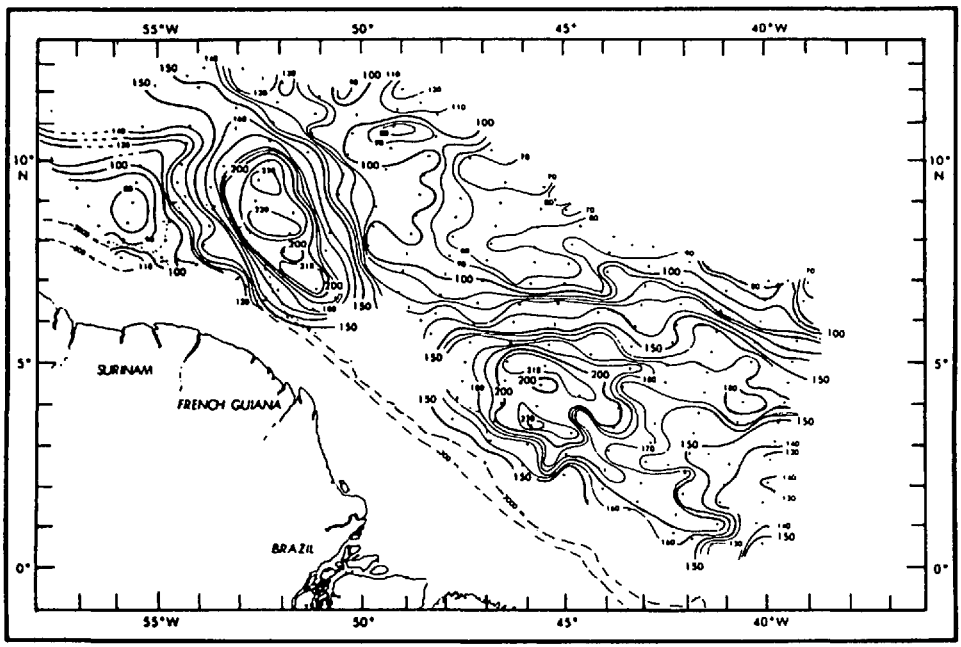

Figure 10. Thermocline depth (m) off the Amazon shelf in boreal summer, determined by AXBT survey. From Bruce and Kerling (1984).

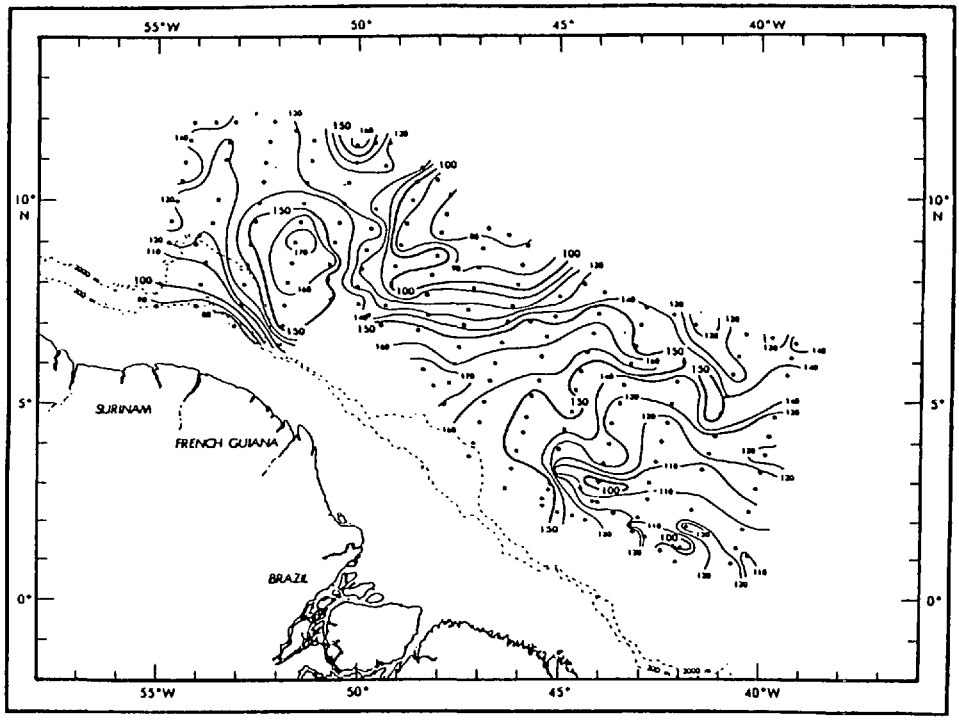

Figure 11. As previous figure, for boreal winter, also from Bruce and Kerling (1984).

over the Demerara Rise, centered at about 8N, 52W, is a permanent feature, except for changes in exact location and in intensity. An "Amazon anticyclone" at about 4 or 5N is also mostly present, although it is weak in winter and looks more like a long offshore ridge than an eddy. There is apparent leakage on the shore side of the Demerara anticyclone into the Guiana Current, past a coastal cyclone in summer, a coastal trough in winter, located near 55W.

A surprising feature of the winter pattern is something like a residual NECC, eastward flow between 7 and 8N. The streamlines bend slightly northward, however, near 45W, and we know from other work that there is no eastward current farther east. The low centered at 10N, 47W is therefore the center of a large cyclonic eddy. Another large cyclonic eddy is present south of the Amazon anticyclone, the latter in this season looking like a long ridge. The survey missed the nearshore portion of the flow pattern between the two anticyclones at about 6N, but a reasonable reconstruction is that the deeper of the NBC streamlines separate from the coast, much as in summer, to recirculate around the Amazon anticyclone.

Returning for a moment to the satellite color images, it is at once clear that the eastward extension of the coastal waters in winter is most likely due to the entrainment of NBC water into the eddies, and the "residual" NECC, rather than to the return of

water carried eastward by the NECC in the previous summer. The complex eddy field in this region is certainly able to distribute the Amazon water over a wide area, a fact noted many years ago by Ryther *et al.* (1967).

c. Inferences from critical point models. Suppose now that summer conditions in the region of the Amazon and Demerara anticyclones are realistically modeled by water masses of different potential vorticity in contact, resulting in boundary and internal stagnation points with properties as discussed above. On the shore side of the apparent stagnation point near 6N one must postulate a cyclonic bulge in the NBC, perhaps even a cyclonic eddy, with a center depth comparable to the center depth of the basin-wide cyclonic gyre, about 70 m. The two anticyclones have comparable center depths, about 220 m. These may be taken to be the rest depths h_1 and h_2 of the water masses in contact.

According to the model results, the stagnation point depth should be 145 m. This is consistent with observed depths. With a Coriolis parameter of $f = 1.5 \times 10^{-5}\,s^{-1}$ and a surface layer buoyancy of $\epsilon g = 2.5 \times 10^{-2}\,m\,s^{-2}$ one calculates $\psi_1 = -27.5$ sv, $\psi_2 = 8.75$ sv (sv = sverdrup = $10^6\,m^3s^{-1}$). If the cyclonic turn on the shore side is just a bulge of the NBC, then ψ_2 is leakage transport into the Guiana Current. Whether bulge or cyclonic eddy, the high potential vorticity of this fluid mass must be attributed to mixing with coastal waters. The southward transport in the nearshore leg of the basin-wide cyclonic gyre should be also some 9 sv. This is much less than the northward transport in the interior of this gyre calculated from the wind stress: about 17 sv according to Hellerman and Rosenstein (1983). Boyd (1986) has found a similarly weak southward flow in what is effectively the Western Boundary Current of the basin-wide cyclonic gyre. Mass balance then requires that the NECC feed the northward interior flow. Float tracks indeed confirm the existence of a direct pathway from the NBC to the NECC, then northward, and back westward in the NEC (Richardson and Reverdin, 1987).

Figure 12 summarizes the inferences from the stagnation point model in a mass balance scheme representing summer conditions. Of the 36 sv entering along the coast from the south with the NBC, 19 sv recirculate, 9 sv continue along the coast as leakage (or Guiana Current), and 8 sv reach the NEC via the interior circulation of the cyclonic gyre. The recirculation takes place fairly close to the western boundary, as part of the Amazon anticyclone. The NECC then transports a total of 17 sv eastward, in accordance with direct estimates from hydrographic sections, and as required by the mass balance of the cyclonic gyre. The Demerara anticyclone recirculates the massive quantity of 28 sv.

West of the Demerara anticyclone the Guiana Current separates from the coast, as another coastal cyclone blocks its way. A model calculation for the apparent boundary stagnation point at 7N, 54W yields similar but somewhat smaller transports than found at the interior stagnation point at 6N, $\psi_1 = -21.4$ sv, $\psi_2 = 7.8$ sv. Change of the

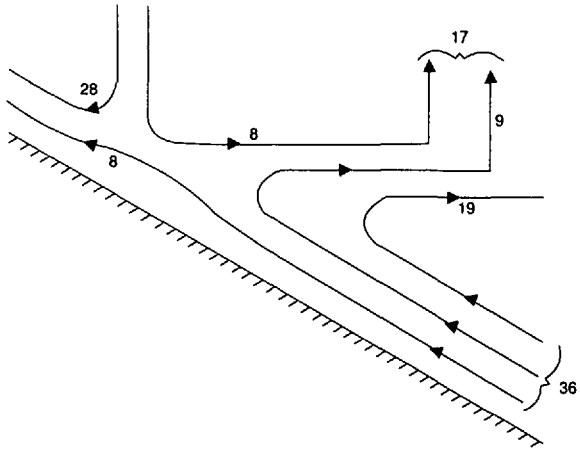

Figure 12. Circulation scheme around stagnation points off the Brazilian coast derived from critical point analysis.

Coriolis parameter is mainly responsible for the difference in the estimates, exposing the limitations of the simple models used.

Winter conditions at the stagnation point near 6N are modeled by $h_1 = 170$ m, $h_2 = 90$ m, $H = 130$ m and lead to transports of $\psi_1 = -11.3$ sv, $\psi_2 = 6$ sv. The latter is again leakage into the Guiana Current, the former recirculation around the Amazon anticyclone. There is no reason to suppose a second pathway to the NEC in this season.

The quantitative transport estimates are of course fairly "soft." However, it is interesting to point out that the 36 sv inflow from the South should reach critical speed at about 3°30'N, just where the streamlines of the Amazon anticyclone begin to separate from the coast. This suggests that the role of the Amazon anticyclone is to operate as a hydraulic control section, restricting the escape rate of warm water from the equatorial pool to what can be transported away by subcritical flow.

The question, how much water escapes northward from that pool, and how much recirculates, is important for the mass balance of equatorially formed warm water. In a study of this mass balance (Csanady, 1987), I have used an ad-hoc parameterization scheme for the escape rate, setting it proportional to the square of the thermocline depth at the western boundary, and to the reciprocal of the Coriolis parameter at a supposed northern limit of the westward equatorial surface drift. A hydraulic control section, restricting transport to the critical limit, at a fixed latitude, yields the same functional relationship of escape transport T_e to depth:

$$T_e = \frac{5}{9}\frac{\epsilon g h^2}{2f}. \tag{41}$$

Here, however, the depth h is the center depth of the Amazon anticyclone, not western boundary depth, and the Coriolis parameter f is near $10^{-5}\,s^{-1}$, corresponding to the low

latitude of the control section, rather than to the latitude of a supposed boundary of an arbitrary equatorial basin.

Acknowledgments. This work was supported by the National Science Foundation under a grant entitled: The North Brazil Current: its role in the equatorial heat and mass balance. Mr. Songjie Liang assisted with the calculations. A lecture by Professor A. D. Kirwan inspired my attempts at using Goldsbrough expansions; he also kindly drew my attention to Perry and Chong's article.

APPENDIX 1

Eq. (5) is a cubic for h:

$$h^3 - Bh^2 + K = 0 \tag{A1}$$

where $K = T^2/2$. Putting:

$$h = \frac{B}{3}(1 + 2y) \tag{A2}$$

Eq. (A1) transforms into:

$$4y^3 - 3y + \frac{27K}{2B^3} - 1 = 0 \tag{A3}$$

Let now:

$$y = \cos u \tag{A4}$$

then using:

$$4\cos^3 u = 3\cos u + \cos 3u \tag{A5}$$

Eq. (A3) becomes:

$$\cos 3u = 1 - \frac{27K}{2B^3} \tag{A6}$$

the three roots of which are:

$$u = \frac{1}{3}\cos^{-1}\left(1 - \frac{27K}{2B^3}\right) + \frac{2n\pi}{3} \tag{A7}$$

with $n = 0$, 1, or 2, $n = 1$ yielding negative h, $n = 2$ supercritical flow. The remaining root is:

$$h = \frac{B}{3}\left(1 + 2\cos\left[\frac{1}{3}\cos^{-1}\left(1 - \frac{27K}{2B^3}\right)\right]\right). \tag{A8}$$

APPENDIX 2

Given that both velocity components vanish at a stagnation point, an obvious approach is to expand them in power series. Let the starting terms of such series be:

$$\begin{aligned} u &= ax + by \\ v &= cx + dy \end{aligned} \tag{A9}$$

the stagnation point being at the origin. Following Goldsbrough's (1930) approach one may try to satisfy the equations of motion exactly by this limited expansion. Substituting Eq. (A9) into the equations of motion (Eq. 1 of the main text), one finds linear functions of x and y on the left, derivatives of h on the right. A quadratic form for h is thus indicated:

$$h = 1 - \frac{jx^2}{2} - \frac{ky^2}{2} - lxy. \tag{A10}$$

Substitution into the continuity equation reveals that the following relations between the constants must be satisfied:

$$\begin{aligned} a + d &= 0 \\ aj + cl &= 0 \\ bl + dk &= 0 \\ bj + ck &= 0. \end{aligned} \tag{A11}$$

The first of these relationships implies that the flow is along depth contours:

$$\mathbf{u} \cdot \nabla h = 0 \tag{A12}$$

which constitutes a severe limitation on the possible flow patterns. Direct integration of the equations of motion now yields the constants j, k, and l in terms of the originally introduced a, b, and c (noting that $d = -a$):

$$\begin{aligned} j &= a^2 + bc - c \\ k &= a^2 + bc + b \\ l &= a. \end{aligned} \tag{A13}$$

Suppose now that $a = 0$. The conditions written down in Eq. (A11) can then be satisfied if either $bc = 0$, or $b + c = 0$. In the former case let $b = 0$; then only the v component of the velocity remains, and with it a simple "ridge or trough" pressure field:

$$\begin{aligned} v &= cx \\ h &= 1 + \frac{cx^2}{2} \end{aligned} \tag{A14}$$

with c positive or negative. If, on the other hand, $b + c = 0$, one finds the thermocline topography shaped as a "bowl" or a "mound":

$$u = by \qquad v = -bx$$
$$h = 1 - \frac{b - b^2}{2}(x^2 + y^2). \tag{A15}$$

If now $a \neq 0$, the conditions in Eq. (A11) require that $a^2 = -bc$, which eventually leads again to the ridge and trough solution, the ridge or trough line oriented at a slope of $-a/b$. Perry and Chong (1987) term the corresponding solution without Coriolis force "pure shear," the equivalent of a bowl or a mound "solid body rotation."

Although the Goldsbrough expansions lead only to a limited class of steady flow patterns, those patterns are undoubtedly realistic, indeed familiar from weather maps, as ridge or trough lines, and centers of a cyclone or anticyclone. It is illuminating to follow up how the streamfunction, the potential vorticity and the Bernoulli function behave in them. The ridge and trough case is the simpler example:

$$\psi = -\frac{cx^2}{2} - \frac{c^2x^4}{8}$$
$$P = \frac{c + 1}{1 + \frac{cx^2}{2}} \tag{A16}$$
$$B = 1 + \frac{cx^2}{2} + \frac{c^2x^2}{2}.$$

The streamfunction and the potential vorticity are both seen to be more complex functions than velocity or depth. All three, ψ, P, and B, are even functions of the coordinates, if the velocity components are odd functions, as one can readily see from the definitions.

None of the above exact solutions resembles the saddle pattern required to model flow around a stagnation point. One might try to find such a pattern by looking for a solution asymptotically valid as $x, y \to 0$. The example of the exact solutions above suggests that the streamfunction should be quadratic in the coordinates: the streamlines are then hyperbolae. The corresponding power series expansion of the streamfunction may be written:

$$\psi = \frac{by^2}{2} - \frac{cx^2}{2} + O(x^4, y^4) \tag{A17}$$

with $bc > 0$. This is closely analogous to the ridge and trough solution. In view of Eqs. (4) and (6a) the potential vorticity and Bernoulli function have the expansions:

$$P = P_0 + \gamma\psi + O(\psi^2)$$
$$B = 1 - P_0\psi - \gamma\psi^2/2 + O(\psi^3) \tag{A18}$$

with $\gamma = \text{const}$. If second order terms in x and y only are retained in Eq. (A17), the velocity, depth and vorticity are calculated to be:

$$\begin{gathered} u = by/h \qquad v = cx/h \\ h = 1 - (P_0 + b)by^2/2 + (P_0 - c)cx^2/2 \\ \zeta = c - b. \end{gathered} \tag{A19}$$

The terms neglected in u and v are of the third order in x, y, in depth of the fourth order, but in vorticity of the second order. The expansions written down here are valid if they satisfy conservation of potential vorticity:

$$(1 + \zeta)/h = P_0 + \gamma(by^2/2 - cx^2/2) + \cdots \tag{A20}$$

With ζ known only to zeroth order, this equation can only be satisfied to the same order, by setting:

$$P_0 = 1 - b + c. \tag{A21}$$

Calculations have shown a fourth order solution to be little better than the second order one, as to its range of validity, both only good to order 0.3 in nondimensional distance from the origin. Comparing Eq. (A21) with Eq. (15) it is clear that this asymptotically valid saddle solution describes the flow in a small neighborhood of the origin where the potential vorticity is homogenized to $P_0 = (P_1 + P_2)/2$. The x, y axes are the bisectors and the inclination of the separation streamlines against one of the axes is $\alpha/2$, so that $c/b = \tan(\alpha/2)$. With the aid of relationships developed in section 3 the value of c and b may be found for any prescribed r:

$$\begin{gathered} c - b = \frac{(r-1)^2}{4r} \\ \frac{c}{b} = \frac{1}{\sqrt{r}}\left(\frac{2\sqrt{r}+1}{2\sqrt{r}+r}\right). \end{gathered} \tag{A22}$$

Thus the homogenized region streamlines can also be determined from the ratio of potential vorticities. Figure A1 shows the streamlines and depth contours calculated for constants $c = -0.221$ and $b = -0.554$, corresponding to a depth ratio of $r = 3$.

The figure illustrates that in the saddle model the depth contours do not coincide with the streamlines. Instead, $h + \psi$ is constant in concentric circles, forming a mound if represented by a surface. The mound part of the pressure field is much the same as found around a stagnation point without earth rotation. Its function is to decelerate the flow approaching the stagnation point, accelerate it upon leaving. To second order in distance the pressure field is thus a simple superposition of a cyclostrophic and a no-rotation field. As Figure A1 shows, the effect of the superposition is to expand the depth contours of the anticyclonic sectors beyond the separation streamlines, compress those of the cyclonic ones.

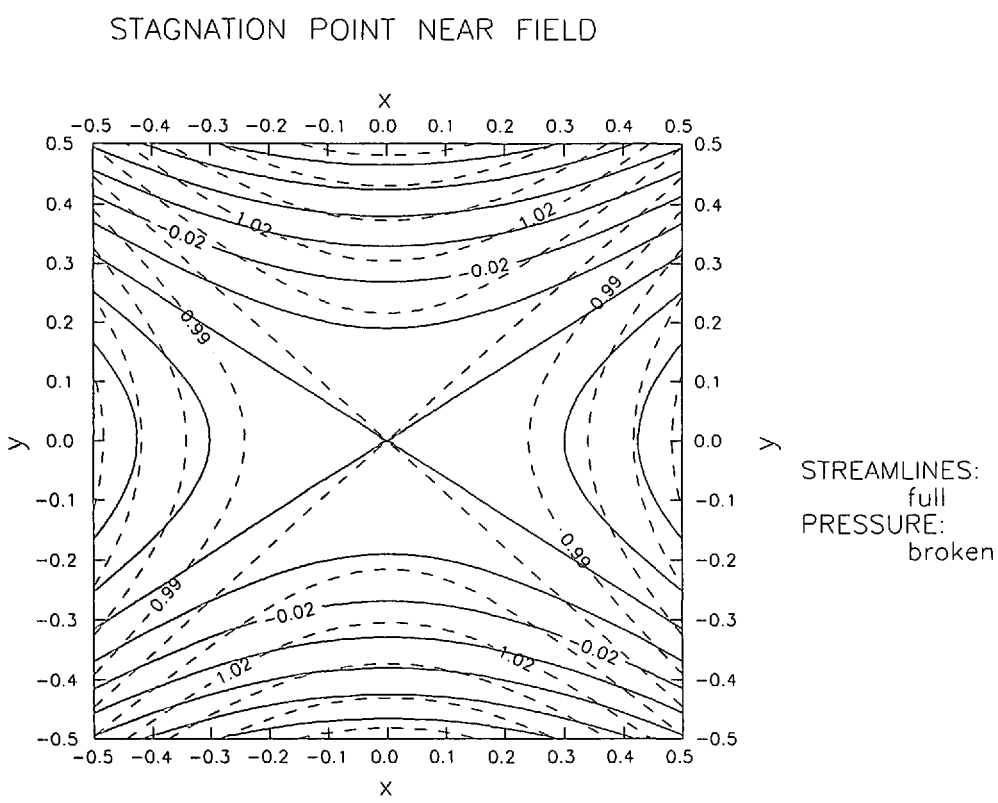

Figure A1. Streamlines (full) and constant depth contours (broken) around saddle stagnation point. Constants have been determined for a depth ratio r = 3, scaled potential vorticity $P = 1.33$, and are $b = -0.554$, $c = -0.221$.

APPENDIX 3

The homogeneous Eq. (34) is satisfied by:

$$\psi = f(r) \cos(n\phi) \qquad n = 0, 1, 2, 3, \ldots \tag{A23}$$

provided that:

$$f(r) = I_n(r), K_n(r).$$

Here r, ϕ are polar coordinates. The boundary condition $\psi = -1$ on the walls of a wedge of included angle α may be satisfied by a series of Bessel functions I_n, using a result listed by Abramowitz and Stegun (1964), p. 376. One finds:

$$-\psi = I_0(r) - 2I_2(r)\frac{\cos(2\phi)}{\cos(\alpha)} + 2I_4(r)\frac{\cos(4\phi)}{\cos(2\alpha)} - 2I_6(r)\frac{\cos(6\phi)}{\cos(3\alpha)} + \cdots \tag{A24}$$

Along the bisector, $\phi = 0$, this tends to infinity at large r.

REFERENCES

Abramowitz, M. and I. A. Stegun. 1964. Handbook of Mathematical Functions. Nat. Bureau of Standards, 1046 pp.

Boyd, J. D. 1986. Thermohaline steps off the northeast coast of South America. Ph.D. dissertation, Texas A.&M. University.

Bruce, J. G. 1987. XBT observations between 10N-10S in the Atlantic from ships of opportunity, complemented by AXBT surveys. Technical Report, WHOI 87-41, Woods Hole Oceanographic Inst., 373 pp.

Bruce, J. G. and J. L. Kerling. 1984. Near equatorial eddies in the North Atlantic. Geophys. Res. Lett., *11,* 779–882.

Bruce, J. G., J. L. Kerling and W. H. Betty III. 1985. On the North Brazilian eddy field. Prog. Oceanogr., *14,* 57–63.

Cabannes, H. 1960. Theorie des Ondes de Choc. Handbuch der Physik, *9,* 162–224, Springer-Verlag.

Courant, R. and D. Hilbert. 1962. Methods of Mathematical Physics, Vol. II. Interscience publishers, 830 pp.

Csanady, G. T. 1985. A zero potential vorticity model of the North Brazilian Coastal Current. J. Mar. Res., *43,* 553–579.

——. 1987. What controls the rate of equatorial warm water mass formation? J. Mar. Res., *45,* 513–532.

Goldsbrough, G. R. 1930. The tidal oscillations in an elliptic basin of variable depth. Proc. Roy. Soc., *A 130,* 157–167.

Hartree, D. R. 1958. Numerical Analysis. Oxford Univ. Press, 302 pp.

Hellerman, S. and M. Rosenstein. 1983. Normal monthly wind stress over the World Ocean with error estimates. J. Phys. Oceanogr., *13,* 1093–1104.

Muller-Karger, F. E., C. R. McClain and P. L. Richardson. 1988. The dispersal of the Amazon's Water. Nature, *133,* 56–59.

Nof, D. 1986. Geostrophic shock waves. J. Phys. Oceanogr., *16,* 886–901.

Parsons, A. T. 1969. A two-layer model of Gulf Stream separation. J. Fluid Mech., *39,* 511–528.

Perry, A. E. and M. S. Chong. 1987. A description of eddying motions and flow patterns using critical-point concepts. Ann. Rev. Fluid Mech., *19,* 125–55.

Richardson, P. L. and G. Reverdin. 1987. Seasonal cycle of velocity in the Atlantic North Equatorial Countercurrent as measured by surface drifters, current meters and ship drifts. J. Geophys. Res., *92,* 3691–3708.

Ryther, J. H., D. W. Menzel and N. Corwin. 1967. Influence of the Amazon River outflow on the ecology of the western tropical Atlantic, I: Hydrography and nutrient chemistry. J. Mar. Res., *25,* 69–83.

Stoker, J. J. 1957. Water waves. Interscience publishers, 567 pp.

Veronis, G. 1981. Evolution of Physical Oceanography, *in* Scientific Surveys in Honor of Henry Stommel, B. A. Warren and C. Wunsch, eds., MIT press, 140–183.

Whitehead, J. A. 1985. The deflection of a baroclinic jet by a wall in a rotating fluid. J. Fluid Mech., *157,* 79–93.

Received: *2 March, 1989;* revised: *23 October, 1990.*